Disorders of the Nervous System

The Neurotoxin DSP-4 Dysregulates the Locus Coeruleus-Norepinephrine System and Recapitulates Molecular and Behavioral Aspects of Prodromal Neurodegenerative Disease

Alexa F. Iannitelli,[1] Michael A. Kelberman,[1] Daniel J. Lustberg,[1] Anu Korukonda,[1] Katharine E. McCann,[1] Bernard Mulvey,[2] Arielle Segal,[1] L. Cameron Liles,[1] Steven A. Sloan,[1] Joseph D. Dougherty,[2,3] and David Weinshenker[1]

[1]Department of Human Genetics, Emory University School of Medicine, Atlanta, GA 30322, [2]Department of Genetics, Washington University School of Medicine, St. Louis, MO 63110, and [3]Department of Psychiatry, Washington University School of Medicine, St. Louis, MO 63110

Abstract

The noradrenergic locus coeruleus (LC) is among the earliest sites of tau and α-synuclein pathology in Alzheimer's disease (AD) and Parkinson's disease (PD), respectively. The onset of these pathologies coincides with loss of noradrenergic fibers in LC target regions and the emergence of prodromal symptoms including sleep disturbances and anxiety. Paradoxically, these prodromal symptoms are indicative of a noradrenergic hyperactivity phenotype, rather than the predicted loss of norepinephrine (NE) transmission following LC damage, suggesting the engagement of complex compensatory mechanisms. Because current therapeutic efforts are targeting early disease, interest in the LC has grown, and it is critical to identify the links between pathology and dysfunction. We employed the LC-specific neurotoxin N-(2-chloroethyl)-N-ethyl-2-bromobenzylamine (DSP-4), which preferentially damages LC axons, to model early changes in the LC-NE system pertinent to AD and PD in male and female mice. DSP-4 (two doses of 50 mg/kg, one week apart) induced LC axon degeneration, triggered neuroinflammation and oxidative stress, and reduced tissue NE levels. There was no LC cell death or changes to LC firing, but transcriptomics revealed reduced expression of genes that define noradrenergic identity and other changes relevant to neurodegenerative disease. Despite the dramatic loss of LC fibers, NE turnover and signaling were elevated in terminal regions and were associated with anxiogenic phenotypes in multiple behavioral tests. These results represent a comprehensive analysis of how the LC-NE system responds to axon/

Significance Statement

Both Alzheimer's disease (AD) and Parkinson's disease (PD) feature early pathology in, and damage to, the noradrenergic locus coeruleus (LC) that coincides with the emergence of prodromal neuropsychiatric symptoms consistent with norepinephrine (NE) dysfunction. Understanding how the locus coeruleus-norepinephrine system becomes dysregulated as it responds to degeneration may be key to developing therapies that ameliorate early disease phenotypes and retard progression. Using the selective locus coeruleus neurotoxin N-(2-chloroethyl)-N-ethyl-2-bromobenzylamine (DSP-4) in mice, we analyzed the response to noradrenergic axon and terminal damage reminiscent of early Alzheimer's disease and Parkinson's disease using molecular, cellular, and behavioral techniques. Our results uncovered aspects of noradrenergic hyperactivity and anxiety-like behavior in mice, suggesting that compensatory mechanisms are engaged in locus coeruleus neurons that may underlie prodromal symptoms of neurodegenerative disease.

terminal damage reminiscent of early AD and PD at the molecular, cellular, systems, and behavioral levels, and provides potential mechanisms underlying prodromal neuropsychiatric symptoms.

Key words: Alzheimer's disease; DSP-4; locus coeruleus; mice; norepinephrine; Parkinson's disease

Introduction

Alzheimer's disease (AD) and Parkinson's disease (PD) are the most common cognitive and motor neurodegenerative disorders, respectively. Both conditions are characterized by abnormal protein accumulation in neurons leading to cellular dysfunction and death. While these disorders differ in their etiology and clinical presentation, early pathology in the brainstem locus coeruleus (LC) is a hallmark of both AD and PD (Weinshenker, 2018). The LC is the primary source of central norepinephrine (NE) and projects to nearly every other brain region (Foote et al., 1983; Berridge and Foote, 1996; Aston-Jones et al., 1999; Poe et al., 2020). LC neurons are the first to accumulate hyperphosphorylated tau in AD (Braak et al., 2011) and they develop aberrant α-synuclein before dopamine neurons of the substantia nigra (SN) in PD (Del Tredici et al., 2002). Although the LC eventually undergoes catastrophic degeneration in both diseases, these neurons can harbor pathology for years before cell death, displaying axon and dendrite loss in initial stages of AD and PD (Halliday et al., 1990; Busch et al., 1997; Theofilas et al., 2017; Doppler et al., 2021; Gilvesy et al., 2022). Combined, these data suggest that LC-NE deficiency contributes to AD and PD. Indeed, experimental lesions of the LC exacerbate neurodegeneration and cognitive deficits in rodent models, and loss of LC integrity correlates with cognitive decline in humans (Weinshenker, 2018; Jacobs et al., 2021b). However, this simplistic view is inconsistent with other data indicating excessive noradrenergic transmission, particularly early in disease. For example, increased levels and turnover of NE have been reported in the CSF of

AD patients (Palmer et al., 1987; Hoogendijk et al., 1999; Henjum et al., 2022). Moreover, because LC activity promotes arousal and stress responses, increased, rather than decreased, NE signaling is consistent with many of the prodromal symptoms of AD and PD including anxiety, depression, agitation, and sleep disturbances (Weinshenker, 2018).

Animal models of AD (Goodman et al., 2021; Kelly et al., 2021; Kelberman et al., 2022) and PD (Butkovich, 2019; Matschke et al., 2022) that recapitulate early LC pathology but lack outright noradrenergic cell death exhibit LC-NE hyperactivity, anxiety-like behavior, and hyperarousal, which can be alleviated with the administration of adrenergic antagonists. Likewise, neuropsychiatric symptoms in AD correlate with high LC signal contrast and respond to blockade of adrenergic receptors (Peskind et al., 2005; Cassidy et al., 2022). We have proposed a more complex model in which damaged LC neurons engage compensatory mechanisms that lead to noradrenergic hyperactivity and contribute to prodromal behavioral phenotypes, followed later by frank LC cell death and NE deficiency that accelerates cognitive decline (Weinshenker, 2018). However, causal relationships between LC damage, cellular and molecular compensatory mechanisms, and prodromal symptoms remain to be investigated and established.

To better understand noradrenergic dysfunction in early neurodegenerative disease and its links to compensatory mechanisms and behavioral abnormalities, we employed the LC-specific neurotoxin N-(2-chloroethyl)-N-ethyl-2-bromobenzylamine (DSP-4), which preferentially damages noradrenergic axons compared with cell bodies (Grzanna et al., 1989; Fritschy and Grzanna, 1991; Zhang et al., 1995). While many groups have reported depletion of NE following DSP-4 administration (Grzanna et al., 1989; Theron et al., 1993; Wolfman et al., 1994; Harro et al., 1999; Szot et al., 2010), it is important to acknowledge some limitations: (1) the effects of DSP-4 are often interpreted as noradrenergic ablation without taking potential compensatory mechanisms into account; (2) most have focused on only a single (or a few) aspect(s) of LC function (e.g., NE abundance *or* axon integrity *or* LC-sensitive behaviors); and (3) many different dosing regimens and species have been used, limiting our ability to integrate the findings into a comprehensive picture of how the LC-NE system responds to damage. Here, we assessed the consequences of DSP-4 administration on molecular, cellular, and behavioral responses of the LC-NE system in parallel. Our results are critical for understanding LC dysfunction in AD and PD, and may provide a foundation for early diagnostic and intervention strategies for these disorders.

Materials and Methods

Animals

Adult male and female C57BL/6 mice were used for all behavioral, electrophysiological, and immunohistochemical

experiments. No statistically significant differences between male and female mice were found in any of the data analyzed, and results were collapsed across sexes. For translating ribosome affinity purification (TRAP) RNA-sequencing experiments, we used male and female transgenic *Slc6a2-eGFP/Rpl10a* mice (B6;FVB-Tg(*Slc6a2-eGFP/Rpl10a*)JD1538Htz/J, The Jackson Laboratory, #031151), which incorporate an EGFP/Rpl10a ribosomal fusion protein into a bacterial artificial chromosome under the *Slc6a2* (NE transporter; NET) promoter to allow for the isolation of polysomes and translating mRNAs specifically from noradrenergic neurons. *Slc6a2-eGFP/Rpl10a* mice were purchased and maintained as hemizygotes on a C57BL/6 background. Mice were group housed with sex-matched and age-matched conspecifics (maximum of five animals per cage) until one week before behavioral testing, and then individually housed for the subsequent week of experimentation until euthanizing. Animals were maintained on a 12/12 h light/dark cycle (lights on at 7 A.M.), and food and water were available *ad libitum*, unless otherwise specified. All experiments were conducted at Emory University in accordance with the National Institutes of Health *Guideline for the Care and Use of Laboratory Animals* and approved by the Emory Institutional Animal Care and Use Committee. Mice were treated with DSP-4 (50 mg/kg, i.p.; Sigma-Aldrich) or vehicle (0.9% NaCl) on days 1 and 7. Electrophysiology and TRAP were conducted on day 14, and behavioral testing commenced on day 14 and ended on day 18.

HPLC

Mice were anesthetized with isoflurane and euthanized by rapid decapitation. The pons, prefrontal cortex (PFC), and hippocampus were rapidly dissected on ice and flash-frozen in isopentane (2-Methylbutane) on dry ice. The samples were weighed and stored at $-80°C$ until processing for HPLC. As previously described (Lustberg et al., 2022), tissue was thawed on ice and sonicated in 0.1 N perchloric acid (10 μl/mg tissue) for 12 s with 0.5-s pulses. Sonicated samples were centrifuged (16-100 rcf) for 30 min at 4°C, and the supernatant was then centrifuged through 0.45-μm filters at 4000 rcf for 10 min at 4°C. For HPLC, an ESA 5600A CoulArray detection system, equipped with an ESA Model 584 pump and an ESA 542 refrigerated autosampler was used. Separations were performed using an MD-150 $\times$ 3.2 mm C18, 3-μm column (Thermo Scientific) at 30°C. The mobile phase consisted of 8% acetonitrile, 75 mM NaH$_2$PO$_4$, 1.7 mM 1-octanesulfonic acid sodium and 0.025% trimethylamine at pH 2.9; 20 μl of sample was injected. The samples were eluted isocratically at 0.4 ml/min and detected using a 6210 electrochemical cell (ESA) equipped with 5020 guard cell. Guard cell potential was set at 475 mV, while analytical cell potentials were -175, 100, 350, and 425 mV. The analytes were identified by the matching criteria of retention time measures to known standards (Sigma). Compounds were quantified by comparing peak areas to those of standards on the dominant sensor.

Immunohistochemistry

Mice were euthanized with an overdose of sodium pentobarbital (Fatal Plus, 150 mg/kg, i.p.; Med-Vet International)

and were transcardially perfused with cold 4% paraformaldehyde (PFA) in 0.01 M PBS. After extraction, brains were postfixed overnight in 4% PFA at 4°C and then transferred to a 30% sucrose/PBS solution for 72 h at 4°C. Brains were embedded in OCT medium (Tissue-Tek) and sectioned by cryostat into 40-um-thick coronal sections at the level of the LC, anterior cingulate cortex (ACC), and hippocampus. Sections were blocked in 5% normal goat serum (NGS) in 0.01 M PBS/0.1% Triton X-100 permeabilization buffer and then incubated for 24 h at 4°C in NGS blocking buffer with primary antibodies listed in Table 1. Following washes in 0.01 M PBS, sections were incubated for 2 h in blocking buffer, including secondary antibodies described in Table 1. After washing, sections were mounted onto Superfrost Plus slides and coverslipped with Fluoromount-G plus DAPI (Southern Biotech).

Quantification

For the catecholaminergic markers NE transporter (NET) and tyrosine hydroxylase (TH), the activity marker activity-regulated cytoskeletal gene (Arc), and the oxidative stress marker 3-nitrotyrosine (3-NT), immunofluorescent micrographs were acquired on a Leica DM6000B epifluorescent upright microscope at 20$\times$ magnification with uniform exposure parameters for each stain and region imaged. Following convention, these images are oriented with the dorsal direction up and the ventral direction down. For glial markers, immunofluorescent images were acquired as z-stack images (10 z-stacks; pitch: 0.1 μm) at 20$\times$ magnification and compressed on a Keyence BZ-X700 microscope system. One representative atlas-matched section was selected from each animal and a standard region of interest (ROI) was drawn for each image to delineate the LC, ACC, and hippocampus. For catecholaminergic and glial markers, image processing and analysis were conducted using the FIJI/ImageJ software. The analysis pipeline included standardized background subtraction, intensity thresholding (Otsu method), and pixel intensity measurements within defined ROIs of the same size (Lustberg et al., 2020a). Furthermore, GFAP$^+$, IBA1$^+$, and S100B$^+$ cells were quantified based on size and shape for glia (50–1000 μm^2, circularity 0.15–1.0; Rorabaugh et al., 2017).

Silver staining

Assessment of degenerating neuronal processes and cell bodies was performed using the NeuroSilver Staining kit II (FD NeuroTechnologies) on fixed, free-floating sections from saline-treated and DSP-4-treated mice ($n = 3$–4 per treatment group). Brain sections (40 μm) were collected by cryostat (Leica) at the level of the LC, ACC, and dentate gyrus (DG). Staining was performed according to the manufacturer's instructions (Kolisnyk et al., 2017; Kumbhare et al., 2017), after which tissue sections were allowed to air-dry overnight on SuperFrost Plus slides (Fisher Scientific). Once dry, sections were cleared for 2 min in CitriSolv xylene substitute (Fisher Scientific) and coverslipped with DPX nonaqueous mounting media (MilliporeSigma). Brightfield micrographs of silver-stained sections were acquired at 20$\times$ magnification using a Keyence BZ-X700 at

Table 1: IHC antibodies

Antibodies	Host	Manufacturer	Catalog #	Dilution
Tyrosine hydroxylase	Chicken	Abcam	ab76442	1:1000
Tyrosine hydroxylase	Rabbit	Pel-Freez	P40101-0	1:1000
Norepinephrine transporter	Mouse	Mab Technologies	NET05-2	1:1000
GFAP	Guinea pig	Synaptic Systems	173004	1:1000
IBA1	Rabbit	FUJIFILM Wako Pure Chemical Corporation	019-19741	1:1000
Nitrotyrosine	Mouse	Abcam	ab125106	1:1000
Arc	Guinea pig	Synaptic Systems	156004	1:1000
NeuroTrace 435/455 blue fluorescent Nissl stain	NA	Thermo Fisher Scientific	N21479	1:500
Alexa Fluor 488 anti-rabbit	Goat	Thermo Fisher Scientific	A-11008	1:500
Alexa Fluor 488 anti-guinea pig	Goat	Thermo Fisher Scientific	A-11073	1:500
Alexa Fluor 568 anti-chicken	Goat	Thermo Fisher Scientific	A-11041	1:500

$20\times$ magnification with uniform light exposure parameters throughout image acquisition.

Cell counts

Coronal tissue sections were processed as described above (Immunohistochemistry) and images were acquired as described for glial markers (see above, Quantification). Using TH as a guide for anatomic LC borders and DAPI as a marker for individual nuclei, sections were atlas-matched and quantified using HALO imaging software (Indica Labs, v3.3.2541.420, FISH/IF v2.1.4). Nine sections were analyzed for each animal ($n = 3$/group), covering most of the LC. The total area analyzed did not differ between the saline-treated and DSP-4-treated groups. Within HALO, nuclei were defined using DAPI, and TH-positive and Nissl-positive nuclei cells were counted and summed across all nine sections for each animal. Comparisons were made between the number of Nissl+ and TH+ nuclei cells in the saline-treated and DSP-4-treated groups.

Translating ribosome affinity purification (TRAP)

To obtain adequate quantities of RNA for sequencing, samples from two six- to eight-month-old, same-sex, and treatment *Slc6a2-eGFP/Rpl10a* mice were pooled to form a biological replicate by dissecting out the hindbrain posterior to the pontine/hypothalamic junction (cerebellum was discarded). Six biological replicates were collected per treatment group. Each replicate was homogenized and TRAP was performed as described (Mulvey et al., 2018), resulting in LC-enriched "TRAP" samples and whole-hindbrain "input" samples. RNA was extracted using Zymo RNA Clean & Concentrator-5 kit, and subsequently sent for library preparation and Illumina sequencing by NovoGene to a minimum depth of 20 million fragments per sample. Forward and reverse sequencing files from each replicate were aligned to the mouse genome (mm10) using STAR alignment, and counts were obtained using FeatureCounts in R Bioconductor. Two samples from saline-treated mice were removed from analysis because the TRAP protocol failed to enrich *Slc6a2* above a 10-fold change, a quality control threshold observed in all other saline-treated samples. All subsequent analysis used R Bioconductor packages. Sequencing data available on NCBI GEO (GSE221404).

To further characterize the gene expression changes, we performed a Weighted Gene Coexpression Network Analysis (WGCNA), as described previously (Zhang and Horvath, 2005; Langfelder et al., 2008). All samples that survived quality control parameters were used to create the co-expression network. Default parameters were primarily used throughout the analysis. The soft threshold power was set at 10, the point in which the scale free topology fit index was above 0.80. Minimum module size was set to 30 genes and modules with >95% similarity were merged, resulting in 159 modules which were then correlated with treatment. We also compared gene expression patterns in our dataset with a repository of gene sets using Gene Set Enrichment Analysis (GSEA 4.2.3; Mootha et al., 2003; Subramanian et al., 2005). Gene set permutation was used, as recommended by GSEA documentation for experiments with fewer than seven samples per group. Other parameters were set to default settings using 1000 gene set permutations and signal-to-noise ranking metric. We downloaded KEGG Pathways from the Molecular Signatures Database, which has 186 gene sets. After filtering for the recommended minimum (15) and maximum (500) gene set size, the remaining 145 gene sets were compared with the expression data from our dataset to calculate the GSEA enrichment score (ES) and to compute significant enrichment.

Electrophysiology

Mice were anesthetized with chloral hydrate (400 mg/kg, i.p.) and placed into a stereotaxic frame. Fur was plucked and an incision was made to expose the skull. Burr holes were drilled over the approximate location of the LC (from bregma, AP: 5.2–5.4; ML: 0.7–1.1).

Recordings were made using 16 channel silicone probes (A1x16-Poly2-5 mm-50s-177-CM16LP, NeuroNexus) that were connected to a μ-series Cereplex headstage (Blackrock Microsystems). Digitized signals were acquired with a 16-channel Cereplex Direct system (Blackrock Microsystems) using a 250-Hz to 5-kHz bandpass filter and a sampling rate of 10 kS/s. Probes were lowered to the approximate location of the LC (DV: -2.7–4.3).

LC units were identified based on standard criteria, including stereotaxic coordinates, biphasic response to foot-pinch/shock, and reduction/cessation of spontaneous activity following injection of the α2-adrenergic receptor agonist clonidine (0.1 mg/kg, i.p.). For each set

of recordings, a 5-min baseline period was collected, and was immediately followed by 10 applications of a contralateral foot-pinch separated by 10 s. Afterwards, 0.5 ms 1 mA footshocks were applied to the contralateral hindpaw separated by 10 s for 5.5 min to assess response to salient/aversive stimuli. LC spikes were manually sorted offline using Blackrock Offline Spike Sorting software.

Electrophysiology data were analyzed using Neuroexplorer. To ensure that recordings were from single units, neurons that had >2% of recorded spikes within a predefined 3-ms refractory period were eliminated from the analysis. Basal firing rate and interspike intervals were calculated based on spikes collected within the 5-min baseline period. Spontaneous burst characteristics (number of bursts, percentage of spikes in a burst, burst duration, spikes per burst, interspike interval within a burst, burst rate, and interburst interval) during baseline was characterized using previously defined criteria derived from dopamine neurons (Grace and Bunney, 1983; Iro et al., 2021). Finally, response to footshock was analyzed in three time windows: immediate (0–60 ms), intermediate (60–100 ms), and long (200–400 ms), as previously described (Hirata and Aston-Jones, 1994).

Behavioral assays

Behavioral assays were performed in the following order, from least to most stressful.

Novelty-induced and circadian locomotion

Individual mice were placed in a Plexiglas arena (10 × 18 × 10 inches) surrounded by a 4 × 8 photobeam grid that records infrared beam breaks (Photobeam Activity System, San Diego Instruments; Lustberg et al., 2020a, b). Two consecutive beam breaks were recorded as an ambulation, and total ambulatory activity was recorded. Mice were left undisturbed in the arena for 23 h. The first hour of the test reflected novelty responses while the remainder of the testing period showed changes in locomotion as a function of circadian cycle. The number and location of ambulations were recorded in 5-min intervals.

Novelty suppressed feeding

Chow was removed from individual home cages 24 h before behavioral testing. Mice were moved to the test room under red light and allowed to habituate for 2 h before the start of the test. Individual mice were placed in a novel arena (10 × 18 × 10 inches) with a single pellet of standard mouse chow located in the center. The latency to feed, operationally defined as grasping and biting the food pellet, was recorded using a stopwatch. Mice that did not feed within the 15-min period were assigned a latency score of 900s (Tillage et al., 2020).

Marble burying

Individual mice were placed in a novel arena (10 × 18 × 10 inches) containing 20 marbles of uniform size and color arranged in a 4 × 5 grid, each on top of 2 inches of lightly pressed cobb bedding. Mice were left undisturbed for 30 min in a brightly lit room. At the end of testing, the mice were placed back into home cages, and the number

of marbles buried were counted by two independent observers. If different scores were reported between observes, the average was taken. A marble was considered buried if at least two-thirds of its height was submerged in the bedding. For each test cage, digital photographs were obtained at uniform angles and distances.

Statistical analyses

Immunohistochemical quantification, stereological cell counting, and HPLC measurements of catechol concentrations were compared between saline-treated and DSP-4-treated groups using a Student's t test in GraphPad Prism. Similarly, behavioral assessment relied on t test comparison between groups for total ambulations in the novelty-induced locomotion assay, latency to feed in the novelty-suppressed feeding task, and number of marbles buried in the marble-burying test. R Bioconductor packages were used for statistical analyses of RNA sequencing data, including differential gene expression (DGE). For electrophysiological recordings, Student's t tests or Mann–Whitney tests were used for comparison of basal firing rates and spontaneous bursting properties between treatment conditions for normally and non-normally distributed data, respectively. A two-way repeated measures ANOVA, with response period as the within subject factor and treatment as the between subject factor, was used to analyze LC response to footshock.

Results

DSP-4 reduces NE content and dysregulates NE turnover in the pons and LC projection fields

To confirm the efficacy and specificity of DSP-4 (two injections of 50 mg/kg, administered one week apart), we assessed tissue levels of catecholamines and their metabolites (Fig. 1). DSP-4 dramatically reduced NE in the pons, where LC cell bodies reside ($t_{(6)} = 17.73$, $p < 0.0001$), as well as in the hippocampus ($t_{(14)} = 3.27$, $p = 0.0056$) and prefrontal cortex (PFC; $t_{(14)} = 3.347$, $p = 0.0048$), two of the primary projection regions of the LC. (Fig. 1a). DSP-4 treatment similarly decreased levels of MHPG, the primary catecholamine metabolite, in the pons ($t_{(6)} = 5.205$, $p = 0.002$), PFC ($t_{(14)} = 2.978$, $p = 0.01$) and hippocampus ($t_{(14)} = 3.140$, $p = 0.0072$; Fig. 1b). Despite the reduction of NE, the rate of turnover (MHPG:NE ratio) was significantly increased in the pons ($t_{(6)} = 2.685$, $p = 0.0363$) and PFC ($t_{(14)} = 2.499$, $p = 0.0255$) compared with saline controls, with a similar trend seen in the hippocampus ($t_{(14)} = 2.049$, $p = 0.0596$), suggesting adaptations in the LC-NE system (Fig. 1c). By contrast, levels of other amine neuromodulators, including dopamine, serotonin, and their respective metabolites, were unchanged in all regions assessed (Table 2), confirming the specificity of this neurotoxin for noradrenergic neurons.

DSP-4 triggers loss of LC fibers and neuroinflammation but not frank cell body degeneration

Consistent with the depletion of tissue NE and canonical findings of LC fiber damage following DSP-4 treatment
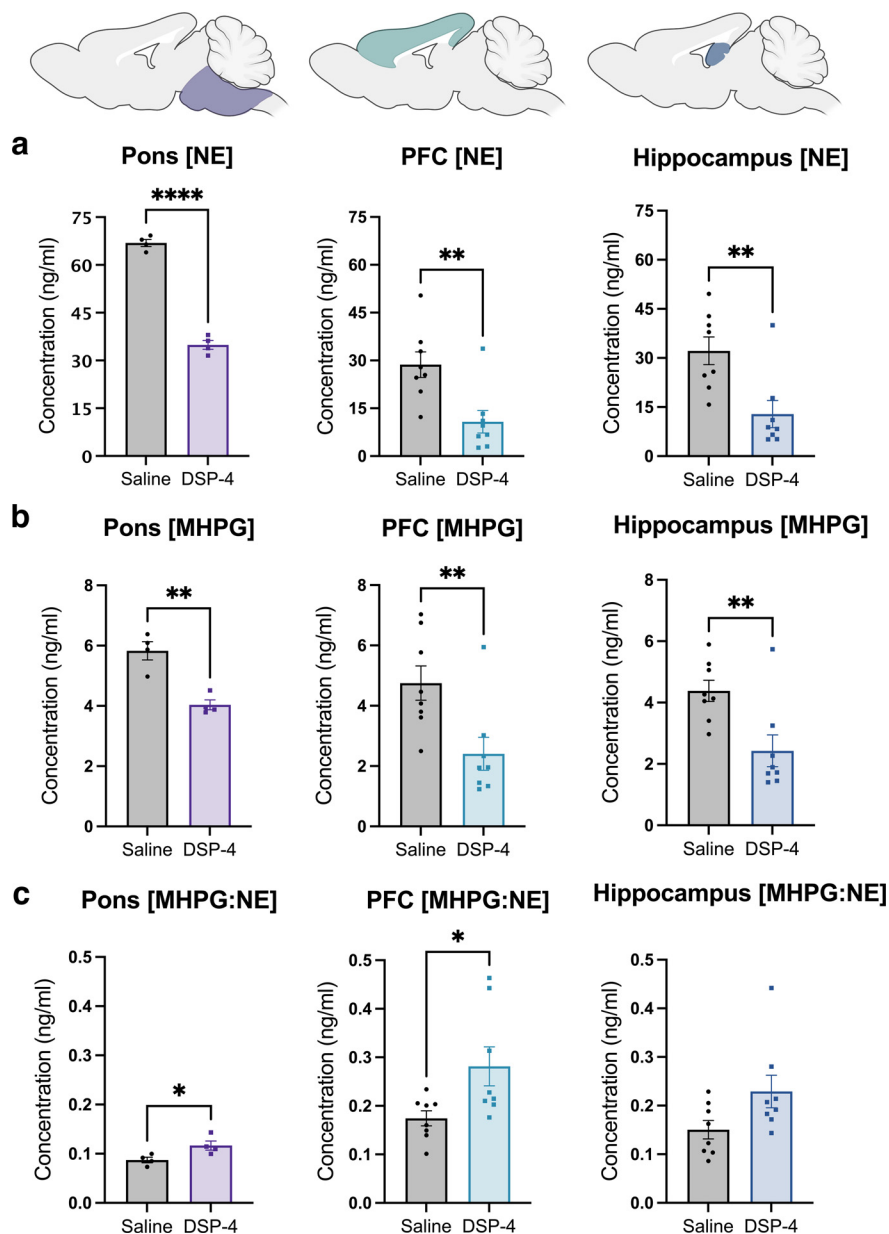
Figure 1. DSP-4 decreases tissue NE and metabolite levels and increases turnover. Mice received saline or DSP-4 (2×50 mg/kg, i.p.), and tissue monoamine and metabolite levels were measured one week later by HPLC in the pons, prefrontal cortex (PFC), and hippocampus (color shaded images at top represent the approximate regions dissected for analysis). DSP-4 significantly decreased NE (**a**) and its primary metabolite MHPG (**b**) in all three brain regions. **c**, NE turnover, defined as the MHPG:NE ratio, was increased in the pons and PFC by DSP-4, with a similar trend in the hippocampus. Data shown as mean $\pm$ SEM, $N = 8$ per group; *$p < 0.05$, **$p < 0.01$, ****$p < 0.0001$.

(Grzanna et al., 1989; Theron et al., 1993; Wolfman et al., 1994; Harro et al., 1999), NET immunoreactivity, a marker of LC axon, dendrite, and terminal integrity, was reduced in the LC ($t_{(6)} = 6.003$, $p = 0.001$), ACC ($t_{(6)} = 13.76$, $p < 0.0001$), and dentate gyrus (DG) region of the hippocampus ($t_{(6)} = 10.23$, $p < 0.0001$) in DSP-4-treated mice compared with controls (Fig. 2a). In contrast, we found that NET immunoreactivity in the bed nucleus of the stria terminalis (BNST), which receives noradrenergic innervation from brainstem A1 and A2 instead of the LC (Aston-Jones et al., 1999), was intact in DSP-4-treated mice (data not

shown), indicating sparing of the ventral noradrenergic bundle and highlighting the specificity of DSP-4-induced damage to LC neurons.

Next, we used silver staining to verify that the loss of NET immunoreactivity reflected LC fiber degeneration and not just a downregulation of NET. Robust silver staining in the LC, ACC, and DG indicated the presence of degenerative processes in the LC and projection regions (Fig. 2b). Finally, we assessed levels of the oxidative stress marker 3-NT in the LC and projection regions and found that it was significantly decreased in the LC following DSP-

Table 2: Tissue monoamine levels measured by HPLC

	Pons		PFC		Hippocampus	
	Saline	DSP-4	Saline	DSP-4	Saline	DSP-4
NE	66.89 ± 1.28	34.91 ± 1.41**	28.69 ± 4.02	10.80 ± 3.56*	32.18 ± 4.23	12.85 ± 4.14*
MHPG	5.83 ± 0.30	4.04 ± 0.16*	4.75 ± 0.57	2.40 ± 0.55*	4.38 ± 0.34	2.42 ± 0.52*
MHPG:NE	0.09 ± 0.01	0.12 ± 0.01*	0.17 ± 0.02	0.28 ± 0.04*	0.15 ± 0.02	0.23 ± 0.03
DA	4.79 ± 0.41	5.27 ± 0.43	52.76 ± 18.95	48.07 ± 22.55	73.84 ± 44.50	92.99 ± 39.37
DOPAC	5.70 ± 0.74	5.94 ± 0.47	27.10 ± 5.67	17.03 ± 4.72	25.50 ± 12.82	28.74 ± 9.26
DOPAC:DA	1.18 ± 0.07	1.15 ± 0.12	0.78 ± 0.12	0.99 ± 0.25	0.98 ± 0.18	0.76 ± 0.19
HVA	6.10 ± 0.39	6.58 ± 0.50	22.35 ± 4.14	16.63 ± 3.25	16.49 ± 7.49	20.44 ± 6.17
5-HT	69.54 ± 8.13	65.91 ± 2.08	42.58 ± 5.87	41.33 ± 4.59	55.86 ± 6.29	51.42 ± 4.22
5-HIAA	64.71 ± 4.47	60.06 ± 2.48	34.01 ± 3.93	26.39 ± 3.06	46.38 ± 5.62	43.25 ± 5.10
5-HIAA:5-HT	1.09 ± 0.15	1.11 ± 0.07	0.86 ± 0.08	0.66 ± 0.06	0.86 ± 0.07	0.87 ± 0.11

Data shown as mean ± SEM, $N = 4$ per group for the pons, and $N = 8$ per group for the PFC and hippocampus; *$p < 0.05$, **$p < 0.01$.

4 administration ($t_{(6)} = 4.746$, $p = 0.0032$), but was increased in the ACC ($t_{(6)} = 4.397$, $p = 0.0046$) and DG ($t_{(6)} = 6.558$, $p = 0.0006$; Fig. 2c).

To determine whether damage resulting from DSP-4 impacted cell body integrity, we performed a count of LC neurons. We quantified DAPI+ cells also positive for TH or NeuroTrace Nissl in the LC. We found no differences in the number of LC neurons in DSP-4-treated mice compared with controls in either analysis (Fig. 2d).

Because neuroinflammation often occurs in response to damage and is a key component of AD and PD pathology (Tansey et al., 2022; Thakur et al., 2022), and glial activation can be impeded by NE signaling (Liu et al., 2019), we assessed immunoreactivity of the astrocyte marker
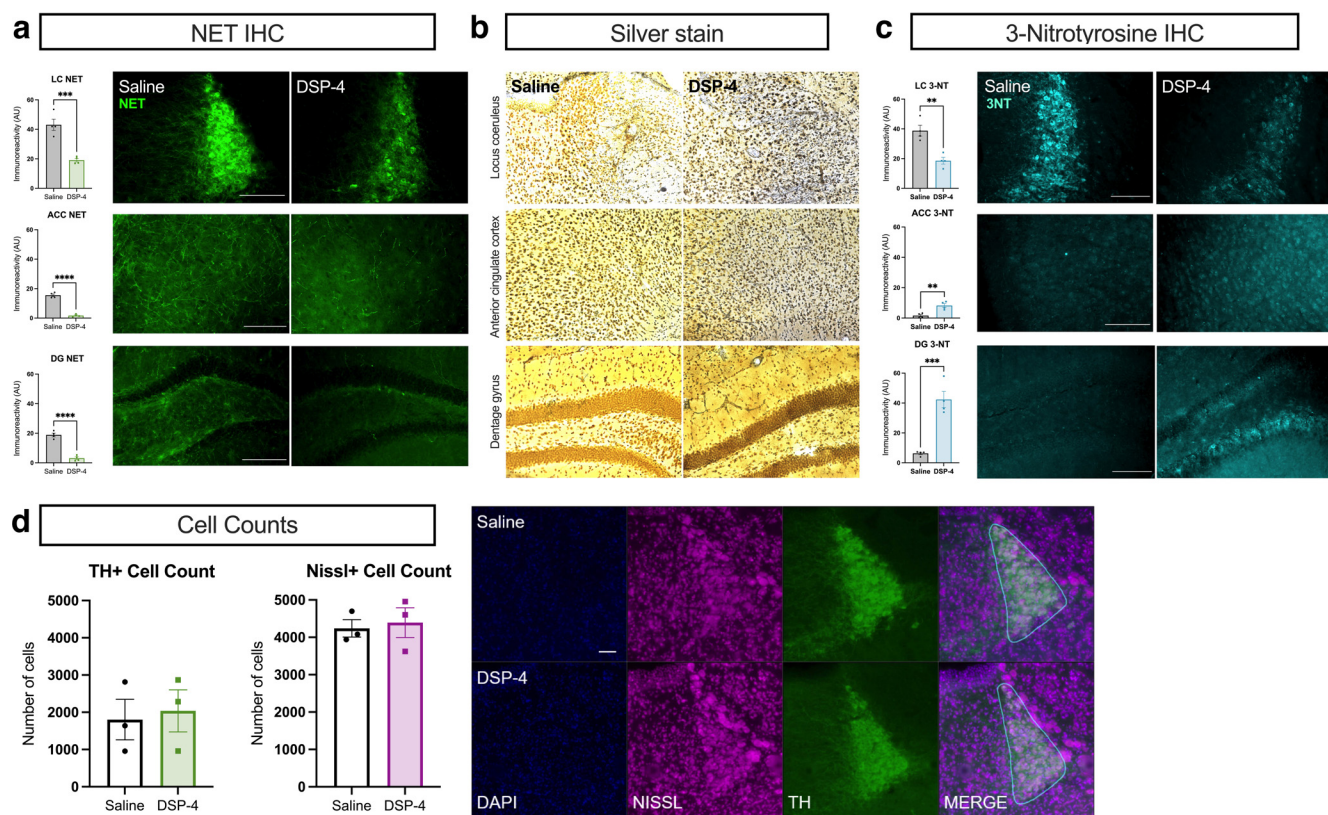

Figure 2. DSP-4 induces degeneration of noradrenergic terminals and oxidative stress but leaves LC cell bodies intact. Mice received saline or DSP-4 (2×50 mg/kg, i.p.) and assessed for locus coeruleus (LC) neuron damage one week later. *a*, DSP-4 results in substantial loss of axon terminals as measured by norepinephrine transporter (NET) immunoreactivity in the dentate gyrus (DG) and anterior cingulate cortex (ACC), with a similar decrease in NET also present in the LC itself. *b*, Representative images of silver-stained brain tissue indicates neurodegenerative processes in the LC, ACC, and DG following DSP-4. *c*, The oxidative stress marker 3-nitrotyrosine (3-NT) was increased in the ACC and DG but decreased in the LC by DSP-4. *d*, Despite NE fiber damage and the evidence of neurodegenerative and oxidative processes following DSP-4, LC cell body number was unaffected as measured by TH and NeuroTrace Nissl immunoreactivity. Images acquired at 20×. Data shown as mean ± SEM, $N = 3–4$ per group; **$p < 0.01$, ***$p < 0.001$, ****$p < 0.0001$.

a   GFAP Immunoreactivity
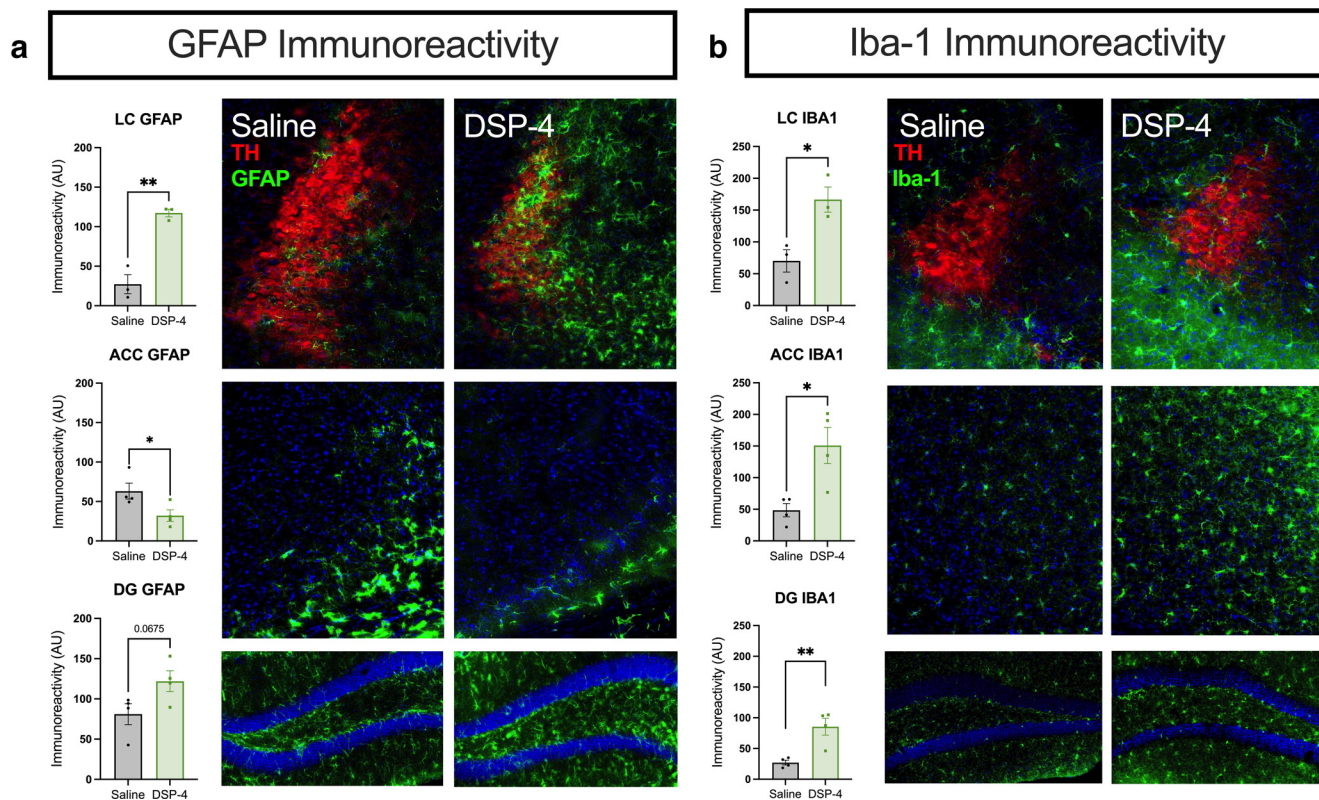

b   Iba-1 Immunoreactivity

Figure 3. DSP-4 alters astrocyte and microglia activation across the LC-NE system. Mice received saline or DSP-4 (2 × 50 mg/kg, i.p.) and assessed for neuroinflammation one week later. **a**, Astrocyte reactivity, as measured by GFAP immunostaining, was significantly increased in the locus coeruleus (LC) with a trend in the dentate gyrus (DG) following DSP-4 treatment, while the anterior cingulate cortex (ACC) showed a decreased astrocytic response. **b**, Microglial response, indicated by Iba-1 immunoreactivity, was increased across all regions assessed. Images acquired at 20×. Data shown as mean ± SEM, N = 3–4 per group; *$p < 0.05$, **$p < 0.01$.

GFAP and the microglial marker Iba-1 in the LC and target regions. We observed robust astrocytic ($t_{(4)} = 6.969$, $p = 0.0022$) and microglial ($t_{(4)} = 3.642$, $p = 0.0219$) responses in and around the LC of DSP-4-treated mice compared with controls (Fig. 3). GFAP immunoreactivity was elevated in the DG ($t_{(6)} = 2.227$, $p = 0.0675$), but decreased in the ACC ($t_{(6)} = 2.480$, $p = 0.0478$), and Iba-1 was increased in both the ACC ($t_{(6)} = 3.351$, $p = 0.0154$) and the DG ($t_{(6)} = 4.118$, $p = 0.0062$). These results reveal that damage to the LC and its projections recapitulates key aspects of neuroinflammation and neurodegeneration in AD and PD.

DSP-4 treatment leads to molecular but not cellular dysfunction in LC cell bodies

The marked reduction in NET immunoreactivity (Fig. 2a) in the LC without the loss of cell bodies (Fig. 2d) suggested that dysregulation of noradrenergic markers may be occurring first on a molecular level. To assess this, we expanded our analysis to the entire LC transcriptome as a complement to our immunohistochemical staining of specific protein markers. We employed a *Slc2a6-Rpll10-eGFP* line for specific targeting of noradrenergic neurons through TRAP (Mulvey et al., 2018). We observed robust enrichment of LC genes in our TRAP samples compared

with input (Fig. 4a and data not shown), indicating the successful implementation of this technique. Next, we assessed differentially expressed genes (DEGs) between replicate samples from the DSP-4 treatment and saline control groups. Most notably, we saw a marked downregulation of multiple noradrenergic function and specification genes, including *Slc6a2* (NET; logFC = −1.5032, $p < 0.0001$), *Th* (logFC = −0.7850, $p = 0.0006$), *Dbh* (logFC = −1.2642, $p < 0.0001$), and *Phox2a* (logFC = −1.0292, $p = 0.0054$), and the LC-enriched neuropeptide *Gal* (logFC = −1.1636, $p < 0.0001$), which is reflective of a loss of LC neuron "identity" following DSP-4 administration (Fig. 4b,c). While only three DEGs reached stringent statistical significance with a false discovery rate (FDR) < 0.1 (*Slc6a2*, *Dbh*, *Gal*), this experiment yielded a substantial list of biologically informative transcripts (Fig. 4c). Further analysis of gene expression networks using WGCNA revealed four modules that were significantly correlated with treatment, one of which included *Dbh*, *Gal*, and *Slc6a2* (Fig. 4d). This module contained 72 genes, including several that are implicated in neurodegenerative diseases (Table 3), suggesting that critical LC genes (*Dbh*, *Gal*, *Slc6a2*) are clustering with neurodegeneration genes in their expression patterns after treatment with DSP-4. Finally, using GSEA to compare the gene expression patterns in our dataset with repositories of known gene sets, we identified 17
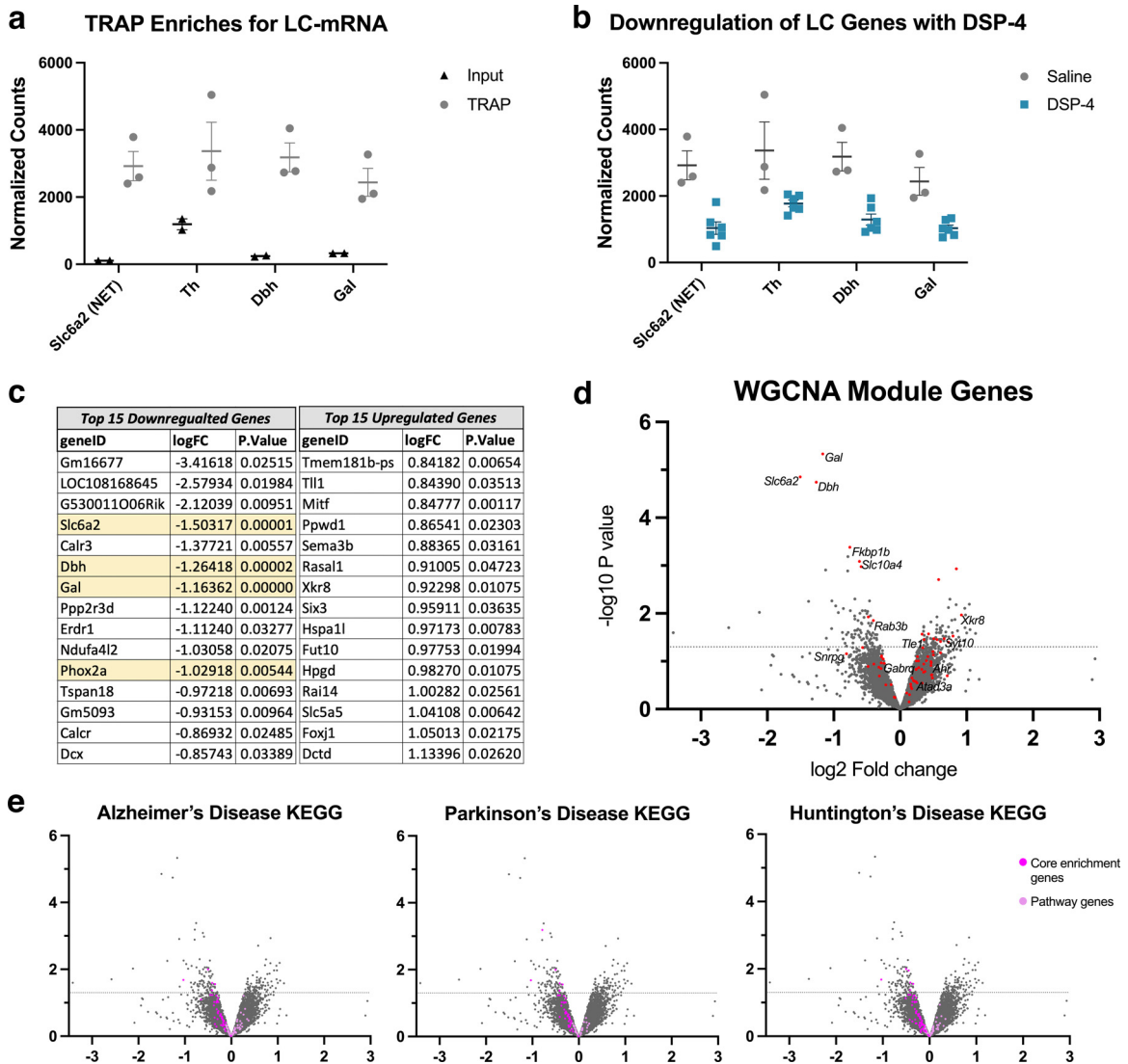
Figure 4. DSP-4 triggers changes in the LC transcriptome. Mice received saline or DSP-4 (2 × 50 mg/kg, i.p.) and LC gene expression was assessed one week later. **a**, TRAP allows for purification of mRNA from LC neurons through immunoprecipitation (TRAP, gray), resulting in enrichment of noradrenergic genes compared with mRNA from the entire hindbrain sample (input, black). **b**, Differential gene expression (DGE) was assessed between DSP-4 (blue) and saline control (gray) TRAP samples, and revealed that noradrenergic-specific genes, including galanin (*Gal*), norepinephrine transporter (*Slc6a2*), dopamine β-hydroxylase (*Dbh*), and tyrosine hydroxylase (*Th*), were among the most significantly and robustly downregulated transcripts in the LC of DSP-4 treated mice. Data for **a** and **b** shown as mean $\pm$ SEM, $N = 2$–6 per group. **c**, List of top 15 downregulated and top 15 upregulated DGE, sorted by fold change (logFC) with $p < 0.05$. **d**, Volcano plot of all filtered, normalized genes (~11,500) with genes from WGCNA-defined module in red. Labeled genes from this module are those of interest based on published connections to neurodegenerative disease. **e**, Volcano plots (as shown in **d**) highlighting genes from three significantly enriched KEGG pathways in our LC data, with GSEA-identified "core enrichment genes" colored magenta, and remaining pathway genes colored light pink.

KEGG pathways that were significantly enriched in our dataset, including oxidative phosphorylation [enrichment score (ES) = −0.53, $p < 0.001$], lysosome (ES = 0.41, $p = 0.006$), pathways in cancer (ES = 0.35, $p = 0.004$), melanogenesis (ES = 0.44, $p = 0.023$), and cytokine-cytokine receptor interaction (ES = 0.45, $p = 0.025$). Notably, the pathways for PD (ES = −0.49, $p < 0.001$), AD (ES = −0.37, $p = 0.037$), and Huntington's disease (ES = −0.45, $p = 0.002$) were significantly negatively correlated with treatment, and further investigation revealed that many of the core enrichment genes in these pathways are similarly downregulated

in clinical neurodegenerative diseases and after DSP-4 treatment in mice (Fig. 4e).

Next, we investigated whether these molecular changes in LC neurons after DSP-4 treatment were accompanied by cellular changes. LC neurons are tonically active, show elevated tonic activity during stress, and exhibit "bursting" activity in response to salient and novel stimuli (Valentino, 1988; Vankov et al., 1995; Curtis et al., 1997; McCall et al., 2015). To determine whether DSP-4-induced molecular dysregulation impacted cellular activity, *in vivo* electrophysiology under anesthesia was conducted to measure

Table 3: Highlighted genes from WGCNA shown in Figure 4

Gene ID	logFC	p value	Gene name and citations
Slc6a2	−1.5032	1.41E-05	*Norepinephrine transporter*, LC enriched gene downregulated in DSP-4 mice
Dbh	−1.2642	1.81E-05	*Dopamine beta-hydroxylase*, LC enriched gene downregulated in DSP-4 mice
Gal	−1.1636	4.67E-06	*Galanin*, LC enriched gene downregulated in DSP-4 mice
Snrpg	−0.8073	0.0698	*Small nuclear ribonucleoprotein polypeptide G*, downregulated in DSP-4 mice; potential AD biomarker (Tao et al., 2020; Du et al., 2021)
Fkbp1b	−0.7567	0.0004	*FK506 binding protein 1B*, downregulated in DSP-4 mice; linked to calcium dysfunction in aging (Gant et al., 2014, 2015)
Slc10a4	−0.613	0.0008	*Solute carrier family 10 member 4*, downregulated in DSP-4 mice; possible links to AD brain pathology (Popova and Alafuzoff, 2013)
Rab3b	−0.4018	0.0141	*Ras-related protein Rab-3B*, downregulated in DSP-4 mice; involved in dopamine vesicular intake
Gabrq	−0.2844	0.1076	*GABA type A receptor subunit theta*, downregulated in DSP-4 mice; associated with behavioral changes in FTD (Gami-Patel et al., 2022)
Atad3a	0.2154	0.2627	*ATPase family AAA domain containing 3A*, upregulated in DSP-4 mice; potential AD biomarker (Zhao et al., 2022)
Tle1	0.3581	0.0351	*TLE family member 1*, transcriptional corepressor, upregulated in DSP-4 mice; potential AD biomarker (Madar et al., 2021)
Ahr	0.4676	0.1082	*Aryl hydrocarbon receptor*, upregulated in DSP-4 mice; potential PD biomarker (Zhou et al., 2021)
Syt10	0.663	0.0335	*Synaptotagmin 10*, upregulated in DSP-4 mice; provides neuroprotection after excitotoxic input (Woitecki et al., 2016)
Xkr8	0.923	0.0107	*XK-related 8*, upregulated in DSP-4 mice; engulfs apoptotic cells

baseline and footshock-evoked firing of LC neurons. There were no differences in the baseline firing rate of LC neurons between treatments (Mann–Whitney $U = 1072$, $p = 0.2312$; Fig. 5), with interspike intervals and spontaneous bursting properties also remaining unchanged (data not shown). There was a main effect of time period in response to footshock such that firing rate of LC neurons decreased in each successive response phase ($F_{(2,176)} = 17.09$, $p < 0.0001$). However, there was no main effect of treatment ($F_{(1,188)} = 2.408$, $p = 0.1243$) or a treatment x time period interaction ($F_{(2,176)} = 0.2655$, $p = 0.7671$) on response to footshock. We conclude that the molecular changes occurring following DSP-4 do not significantly affect LC neuron firing under these conditions.

DSP-4 treatment results in a novelty-induced anxiety phenotype, implying compensatory hyperactivity of LC-NE transmission

AD and PD share several prodromal behavioral symptoms related to affect and arousal, processes known to be regulated by the LC-NE system and sensitive to LC integrity (Weinshenker, 2018). Moreover, cognitive impairment is a diagnostic criterion for AD and is common in later stage PD; thus, we assessed the consequences of DSP-4 on LC/NE-sensitive behaviors that reflect prodromal and cognitive abnormalities in AD and PD. We found that lesioned mice were profoundly more reactive in novelty-induced stress paradigms, which are commonly used to model anxiety and are bidirectionally modulated by NE (Lustberg et al., 2020b). DSP-4-treated mice took significantly longer to consume food in the novelty-suppressed feeding test ($t_{(20)} = 3.158$, $p = 0.0048$), buried more marbles ($t_{(14)} = 4.290$, $p = 0.0007$), and ambulated less during the first hour in a novel cage ($t_{(14)} = 2.999$, $p = 0.0096$) compared with saline-treated controls (Fig. 6). Importantly, DSP-4 treatment had no effect on latency to eat in the home cage or in total ambulations across a 23-h period, suggesting increased anxiety-like behavior rather than a decrease in hunger or general locomotion. Arousal (as assessed by latency to fall asleep following gentle handling) and associative memory (as measured by freezing in a
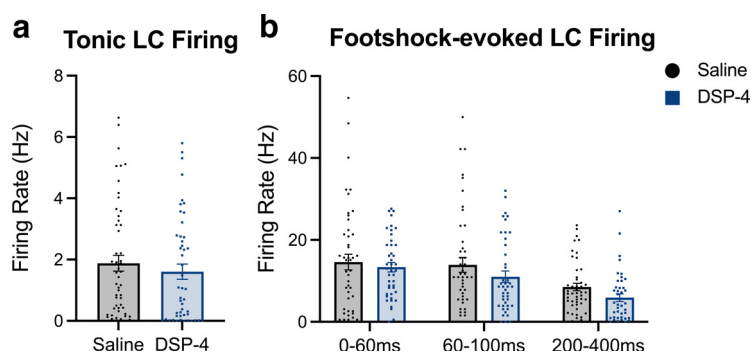

Figure 5. DSP-4 treatment does not alter baseline or footshock-induced LC activity. Mice received saline or DSP-4 (2×50 mg/kg, i.p.) and assessed for locus coeruleus (LC) neuron firing under anesthesia one week later. No differences were found for (***a***) baseline tonic firing rates (in Hertz). ***b***, There was no main effect of treatment on footshock-evoked firing rates of LC neurons 0–60, 60–100, or 200–400 ms following the stimulus. Data shown as mean ± SEM, $N = 5$ mice per group 42–53 neurons/group.
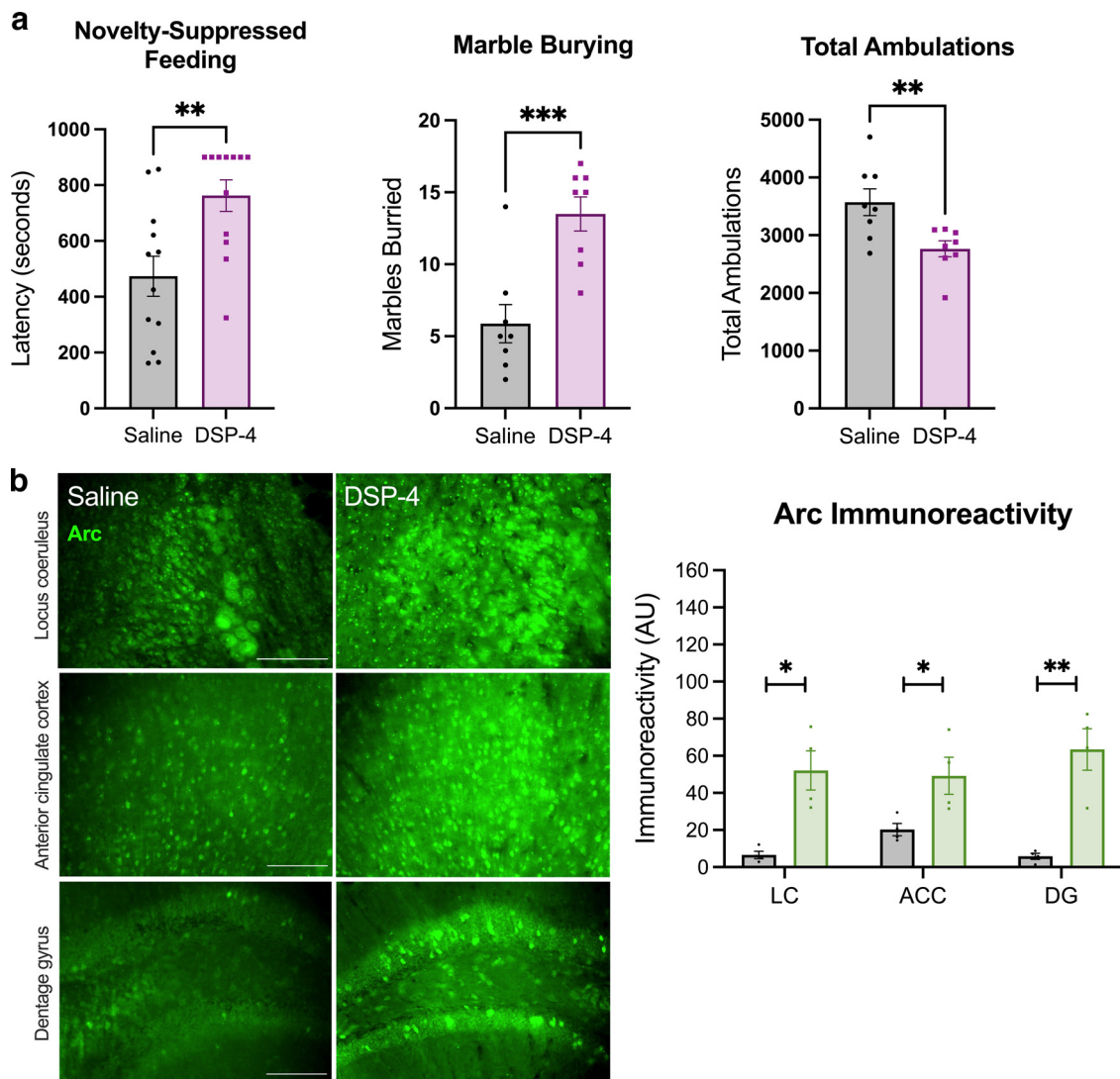
Figure 6. DSP-4 increases novelty-induced anxiety and arc expression. ***a***, DSP-4-treated mice display increased latency to bite the food pellet in the novelty-suppressed feeding test, buried more marbles, and showed fewer ambulations in response to a novel environment ($N = 8$–12 per group). ***b***, Immunoreactivity for the immediate early gene Arc following cage change was reduced in the locus coeruleus (LC) and projection regions (anterior cingulate cortex, ACC; dentate gyrus region of the hippocampus, DG; $N = 3$–4 per group). Images acquired at 20×. Data shown as mean $\pm$ SEM; *$p < 0.05$, **$p < 0.01$, ***$p < 0.001$.

footshock-associated context) did not differ between treatment groups (data not shown).

Elevated novelty-induced anxiety-like behavior is consistent with increased noradrenergic activity (Lustberg et al., 2020a), which was surprising given the profound loss of noradrenergic fibers and NE in LC terminal fields. Our HPLC data indicated increased NE turnover from surviving terminals, and adrenergic receptor supersensitivity has been reported in DSP-4-lesioned animals (Wolfman et al., 1994; Szot et al., 2010). To investigate whether these adaptations are sufficient to boost downstream signaling mechanisms that underlie behavioral reactivity, immunostaining for Arc was quantified following cage change, a mild stressor that is resistant to habituation and sensitive to NE transmission (Vankov et al., 1995; McCall et al., 2015; Takeuchi et al., 2016; Grella et al., 2019; Lustberg et al., 2020a, b; Prokopiou et al., 2022). Arc is an

immediate early gene and neural activity marker that is induced following adrenergic receptor stimulation, and acts as a readout of postsynaptic LC-NE transmission (McIntyre et al., 2005; McReynolds et al., 2014). After cage change, a marked increase in Arc immunoreactivity was observed in the LC ($t_{(6)} = 4.258$, $p = 0.0053$), ACC ($t_{(6)} = 2.755$, $p = 0.0331$), and DG ($t_{(6)} = 5.099$, $p = 0.0022$) of DSP-4-treated mice compared with saline-treated mice (Fig. 6).

Discussion

The present study characterized the impact of DSP-4 on the molecular, cellular, and behavioral levels in mice to comprehensively assess the consequences of damage to LC neurons reminiscent of early stages of AD and PD. The depletion of NE and its metabolite MHPG, as well as the elevated MHPG:NE ratio, by DSP-4 are consistent with

decades of previous research and indicate reduced total NE but increased NE turnover (Jonsson et al., 1981; Logue et al., 1985; Harro et al., 1999; Szot et al., 2010). Immunohistochemical staining following DSP-4 treatment revealed a dramatic reduction of NET in the PFC and hippocampus, which could mean a loss of noradrenergic terminals and/or a downregulation of NET expression. We found evidence for both. NET mRNA in LC neurons was significantly reduced by DSP-4, and silver staining provided evidence for degeneration of axons/terminals in projection regions. Diminished NET immunoreactivity was also observed in the LC of DSP-4-treated mice. To determine whether this was because of a loss of neurons, we counted LC cell bodies (i.e., positive for DAPI and TH or Nissl) and found no effect of DSP-4, which is typical for similar dosing regimens (Lyons et al., 1989; Matsukawa et al., 2003; Szot et al., 2010). Taken together, the loss of NE and NET in terminal regions and pons is indicative of LC axon, terminal, and dendrite degeneration, with the increased MHPG:NE ratio potentially signifying compensatory elevation of NE release from surviving fibers (Jacobs, 2019; van Hooren et al., 2021; Gilvesy et al., 2022).

DSP-4 provoked oxidative stress in the forebrain and a robust neuroimmune response in the both the LC and its projection regions. 3-NT immunoreactivity was elevated in the ACC and DG following DSP-4 administration, providing a link to AD, as LC lesions also increased 3-NT in the cortex of mice that overexpress mutant amyloid precursor protein (Heneka et al., 2006). Paradoxically, the abundance of 3-NT in control LCs was high at baseline relative to the other brain regions and decreased by DSP-4. Catecholamine synthesis and metabolism generate oxidative stress, which could contribute to the high baseline levels of 3-NT in the LC, while the DSP-4-induced reduction may reflect the loss of catecholamine synthetic capacity. Interestingly, lipopolysaccharide-induced 3-NT oxidative stress in the dopaminergic SN that is reminiscent of PD pathology was also attenuated by DSP-4 lesions of the LC (Iravani et al., 2014).

Microglial activation as measured by Iba-1 immunoreactivity was elevated in the LC, ACC, and DG of DSP-4-treated mice compared with controls. GFAP+ reactive astrocytes were increased in the LC and DG of DSP-4 tissue but were suppressed in the ACC. The interplay between neuroinflammation and neurodegeneration is bidirectional, and our experiments with NeuroSilver staining revealed active degenerative processes in both fibers and cell bodies of the LC and its projection regions. Because our analysis was restricted to a single time point when both processes were evident, we cannot know whether one triggered the other. Neuroinflammation and neurodegeneration are key components of AD and PD, and both are exacerbated by ablation of LC-NE in animal models of these disorders and can be ameliorated by pro-noradrenergic therapies in clinical populations (Rommelfanger et al., 2004, 2007; Heneka et al., 2006, 2010; Chalermpalanupap et al., 2018; Song et al., 2019a, b; Levey et al., 2022). Given that we observed no difference in LC cell body number, our DSP-4 dosing regimen appears to represent an early phase of neurodegeneration, which is characterized by

initial loss of noradrenergic innervation before frank LC degeneration in AD and PD (Fritschy et al., 1990; Doppler et al., 2021; Gilvesy et al., 2022).

In AD and PD, LC neurons become dysfunctional early on but persist for many years before cell death. However, almost nothing is known about the molecular changes that drive LC dysfunction before outright degeneration. Because of its small size and neuron number, selective mRNA profiling of the murine LC transcriptome has historically been challenging. To address this gap, we assessed the effects of DSP-4 treatment on the LC transcriptome using TRAP and obtained enrichment of known LC genes such as *Th*, *Slc6a2* (NET), *Dbh*, *Phox2a*, and *Gal* in saline-treated mice, as previously reported (Mulvey et al., 2018). Remarkably, we found that these same genes were downregulated in DSP-4-treated mice, suggesting a deterioration of noradrenergic identity before LC neuron loss. Differential gene expression and down-regulation of NET, *Dbh*, and *Th* are consistent with *in vitro* studies exposing SH-SY5Y cells to DSP-4 (Wang et al., 2014), but opposite of what has been reported in clinical AD, where *Th* and NET are increased in surviving LC neurons (Szot et al., 2006). We speculate that compensatory increases in noradrenergic markers are triggered by the cell loss ubiquitous in late-stage AD, which did not occur in our DSP-4-treated mice. In addition to the disruption in noradrenergic gene expression, we also found several genes associated with neurodegeneration and neurotoxicity that were differentially expressed between our treatment groups. Some of these genes, highlighted in Figure 4 and detailed in Table 3, were also found in the co-expression network module with *Gal*, *Dbh*, and *Slc6a2*. These results were complemented by significant enrichment in gene sets associated with AD, PD, and Huntington's disease, and contribute to the rich array of potential genetic targets for better understanding the early stages of neurodegeneration.

Prodromal AD and PD are characterized by neuropsychiatric abnormalities including anxiety, agitation, depression, and sleep disturbances that appear long before the primary diagnostic symptoms of these diseases (cognitive and motor impairment, respectively). Using a battery of tests to probe these behavioral domains, we found that DSP-4-treated mice displayed increased anxiety-like behavior specific to novelty: they took significantly longer to consume a food pellet, buried more marbles, and had reduced locomotor activity in novel environments. These results are consistent with previous reports that surgical or neurotoxin ablation of the LC in rats induces similar anxiety-like phenotypes that reflect responses to novelty stress (Martin-Iverson et al., 1982; Harro et al., 1995).

LC-NE transmission is triggered by novelty stress, and activation of this system promotes, while inactivation suppresses, novelty-induced anxiety (McCall et al., 2015; Lustberg et al., 2020a, b). Thus, the emergence of anxiety-like behavior in DSP-4-treated mice and AD/PD patients where a dramatic *loss* of noradrenergic fibers and NE is evident creates a paradox and suggests that compensatory mechanisms are engaged in response to LC damage that led to hyperactive NE transmission. We can imagine three potential neuroanatomical/neurobiological

substrates where this compensation may occur: LC cell bodies (e.g., increased neuron firing), LC terminals (e.g., increased NE release from surviving fibers), and/or postsynaptic compartments (e.g., receptor/signaling molecules super-sensitivity).

Using *in vivo* electrophysiology, we detected no differences in the baseline (firing rate, interspike interval, spontaneous bursting properties) or footshock-evoked firing rate of LC neurons. This is consistent with previous reports in DSP-4-treated rats (Szot et al., 2010) but distinct from partial 6-OHDA LC lesions, which increased LC activity in mice (Szot et al., 2016). One important difference is that the 6-OHDA-treated mice had LC neuron loss (~30%), while LC cell bodies remained intact in our study. These results suggest that LC neurons are capable of compensatory increases in firing, but that cell body degeneration is required to trigger this response. By contrast, we did find evidence for increased NE release from surviving fibers. Although we did not measure this directly, metabolite to parent neurotransmitter ratio is a validated proxy for turnover. Despite lower NE and MHPG levels in the lesioned mice, we detected elevated MHPG:NE ratio in the LC and terminal regions, which has been previously reported in DSP-4-treated rodents (Hallman and Jonsson, 1984) and consistent with human AD CSF data (Francis et al., 1985; Hoogendijk et al., 1999; Raskind et al., 1999; Jacobs et al., 2021b). Indeed, high CSF MHPG levels are associated with neuropsychiatric abnormalities in AD (Jacobs et al., 2021a). Thus, despite reduced total NE and MHPG, there may be sparse "hotspots" of dysregulated NE release from surviving fibers that contribute to phenotypes consistent with excessive NE transmission.

Finally, postsynaptic compensatory mechanisms resulting from the loss of LC fibers may be at play. There are many reports of increased adrenergic receptor density following DSP-4 administration (Johnson et al., 1987; Harro et al., 1999), but the consequences on downstream receptor signaling have not been carefully investigated. We performed immunostaining for the immediate early gene Arc, which is a marker for neuronal activity and induced by activation of adrenergic receptors (Essali and Sanders, 2016). Following cage-change stress, Arc immunoreactivity was dramatically elevated in DSP-4-treated tissue compared with controls in the LC and its output regions in the forebrain. We conclude that compensatory changes in NE release from surviving LC terminals and/or postsynaptic adrenergic receptor signaling could contribute the anxiogenic effects of DSP-4, while increases in LC firing do not. These results have important implications for AD and PD, where early LC pathology, damage to noradrenergic fibers, and neuropsychiatric symptoms precede frank LC loss in prodromal disease. In addition, these experiments support the notion that DSP-4 dysregulates, rather than simply ablates, the noradrenergic system, and should act as a caution to researchers employing this neurotoxin as they interpret their results.

References

Aston-Jones G, Rajkowski J, Cohen J (1999) Role of locus coeruleus in attention and behavioral flexibility. Biol Psychiatry 46:1309–1320.

Berridge CW, Foote SL (1996) Enhancement of behavioral and electroencephalographic indices of waking following stimulation of noradrenergic beta-receptors within the medial septal region of the basal forebrain. J Neurosci 16:6999–7009.

Braak H, Thal DR, Ghebremedhin E, Del Tredici K (2011) Stages of the pathologic process in Alzheimer disease: age categories from 1 to 100 years. J Neuropathol Exp Neurol 70:960–969.

Busch C, Bohl J, Ohm TG (1997) Spatial, temporal and numeric analysis of Alzheimer changes in the nucleus coeruleus. Neurobiol Aging 18:401–406.

Butkovich LM, Houser MC, Chalermpalanupap T, Porter-Stransky KA, Eidson LN, De Sousa Rodrigues ME, Oliver DL, Kelly SD, Chang J, Bengoa-Vergniory N, Wade-Martins R, Weinshenker D, Tansey MG (2019) Transgenic mice expressing human alpha-synuclein in noradrenergic neurons develop locus coeruleus pathology and non-motor features of Parkinson's disease. bioRxiv 857987. https://doi.org/10.1101/857987.

Cassidy CM, Therriault J, Pascoal TA, Cheung V, Savard M, Tuominen L, Chamoun M, McCall A, Celebi S, Lussier F, Massarweh G, Soucy JP, Weinshenker D, Tardif C, Ismail Z, Gauthier S, Rosa-Neto P (2022) Association of locus coeruleus integrity with Braak stage and neuropsychiatric symptom severity in Alzheimer's disease. Neuropsychopharmacology 47:1128–1136.

Chalermpalanupap T, Schroeder JP, Rorabaugh JM, Liles LC, Lah JJ, Levey AI, Weinshenker D (2018) Locus coeruleus ablation exacerbates cognitive deficits, neuropathy, and lethality in P301S tau transgenic mice. J Neurosci 38:74–92.

Curtis AL, Lechner SM, Pavcovich LA, Valentino RJ (1997) Activation of the locus coeruleus noradrenergic system by intracoerulear microinfusion of corticotropin-releasing factor: effects on discharge rate, cortical norepinephrine levels and cortical electroencephalographic activity. J Pharmacol Exp Ther 281:163–172.

Del Tredici K, Rüb U, De Vos RA, Bohl JR, Braak H (2002) Where does parkinson disease pathology begin in the brain? J Neuropathol Exp Neurol 61:413–426.

Doppler CEJ, Kinnerup MB, Brune C, Farrher E, Betts M, Fedorova TD, Schaldemose JL, Knudsen K, Ismail R, Seger AD, Hansen AK, Stær K, Fink GR, Brooks DJ, Nahimi A, Borghammer P, Sommerauer M (2021) Regional locus coeruleus degeneration is uncoupled from noradrenergic terminal loss in Parkinson's disease. Brain 144:2732–2744.

Du B, Zhang Y, Liang M, Du Z, Li H, Fan C, Zhang H, Jiang Y, Bi X (2021) N6-methyladenosine (m6A) modification and its clinical relevance in cognitive dysfunctions. Aging (Albany NY) 13:20716–20737.

Essali N, Sanders J (2016) Interdependent adrenergic receptor regulation of Arc and Zif268 mRNA in cerebral cortex. Neurosci Lett 612:38–42.

Foote SL, Bloom FE, Aston-Jones G (1983) Nucleus locus ceruleus: new evidence of anatomical and physiological specificity. Physiol Rev 63:844–914.

Francis PT, Palmer AM, Sims NR, Bowen DM, Davison AN, Esiri MM, Neary D, Snowden JS, Wilcock GK (1985) Neurochemical studies of early-onset Alzheimer's disease. Possible influence on treatment. N Engl J Med 313:7–11.

Fritschy JM, Grzanna R (1991) Selective effects of DSP-4 on locus coeruleus axons: are there pharmacologically different types of noradrenergic axons in the central nervous system? Prog Brain Res 88:257–268.

Fritschy JM, Geffard M, Grzanna R (1990) The response of noradrenergic axons to systemically administered DSP-4 in the rat: an immunohistochemical study using antibodies to noradrenaline and dopamine-beta-hydroxylase. J Chem Neuroanat 3:309–321.

Gami-Patel P, Scarioni M, Bouwman FH, Boon BDC, van Swieten JC, Brain BN, Rozemuller AJM, Smit AB, Pijnenburg YAL, Hoozemans JJM, Dijkstra AA (2022) The severity of behavioural symptoms in FTD is linked to the loss of GABRQ-expressing VENs and pyramidal neurons. Neuropathol Appl Neurobiol 48:e12798.

Gant JC, Blalock EM, Chen KC, Kadish I, Porter NM, Norris CM, Thibault O, Landfield PW (2014) FK506-binding protein 1b/12.6: a

key to aging-related hippocampal Ca2+ dysregulation? Eur J Pharmacol 739:74–82.

Gant JC, Chen KC, Kadish I, Blalock EM, Thibault O, Porter NM, Landfield PW (2015) Reversal of aging-related neuronal Ca2+ dysregulation and cognitive impairment by delivery of a transgene encoding FK506-binding protein 12.6/1b to the hippocampus. J Neurosci 35:10878–10887.

Gilvesy A, Husen E, Magloczky Z, Mihaly O, Hortobágyi T, Kanatani S, Heinsen H, Renier N, Hökfelt T, Mulder J, Uhlen M, Kovacs GG, Adori C (2022) Spatiotemporal characterization of cellular tau pathology in the human locus coeruleus-pericoerulear complex by three-dimensional imaging. Acta Neuropathol 144:651–676.

Goodman AM, Langner BM, Jackson N, Alex C, McMahon LL (2021) Heightened hippocampal β-adrenergic receptor function drives synaptic potentiation and supports learning and memory in the TgF344-AD rat model during prodromal Alzheimer's disease. J Neurosci 41:5747–5761.

Grace AA, Bunney BS (1983) Intracellular and extracellular electrophysiology of nigral dopaminergic neurons–3. Evidence for electrotonic coupling. Neuroscience 10:333–348.

Grella SL, Neil JM, Edison HT, Strong VD, Odintsova IV, Walling SG, Martin GM, Marrone DF, Harley CW (2019) Locus coeruleus phasic, but not tonic, activation initiates global remapping in a familiar environment. J Neurosci 39:445–455.

Grzanna R, Berger U, Fritschy JM, Geffard M (1989) Acute action of DSP-4 on central norepinephrine axons: biochemical and immunohistochemical evidence for differential effects. J Histochem Cytochem 37:1435–1442.

Halliday GM, Li YW, Blumbergs PC, Joh TH, Cotton RG, Howe PR, Blessing WW, Geffen LB (1990) Neuropathology of immunohistochemically identified brainstem neurons in Parkinson's disease. Ann Neurol 27:373–385.

Hallman H, Jonsson G (1984) Monoamine neurotransmitter metabolism in microencephalic rat brain after prenatal methylazoxymethanol treatment. Brain Res Bull 13:383–389.

Harro J, Oreland L, Vasar E, Bradwejn J (1995) Impaired exploratory behaviour after DSP-4 treatment in rats: implications for the increased anxiety after noradrenergic denervation. Eur Neuropsychopharmacol 5:447–455.

Harro J, Pähkla R, Modiri AR, Harro M, Kask A, Oreland L (1999) Dose-dependent effects of noradrenergic denervation by DSP-4 treatment on forced swimming and beta-adrenoceptor binding in the rat. J Neural Transm (Vienna) 106:619–629.

Heneka MT, Ramanathan M, Jacobs AH, Dumitrescu-Ozimek L, Bilkei-Gorzo A, Debeir T, Sastre M, Galldiks N, Zimmer A, Hoehn M, Heiss WD, Klockgether T, Staufenbiel M (2006) Locus ceruleus degeneration promotes Alzheimer pathogenesis in amyloid precursor protein 23 transgenic mice. J Neurosci 26:1343–1354.

Heneka MT, Nadrigny F, Regen T, Martinez-Hernandez A, Dumitrescu-Ozimek L, Terwel D, Jardanhazi-Kurutz D, Walter J, Kirchhoff F, Hanisch UK, Kummer MP (2010) Locus ceruleus controls Alzheimer's disease pathology by modulating microglial functions through norepinephrine. Proc Natl Acad Sci U S A 107:6058–6063.

Henjum K, Watne LO, Godang K, Halaas NB, Eldholm RS, Blennow K, Zetterberg H, Saltvedt I, Bollerslev J, Knapskog AB (2022) Cerebrospinal fluid catecholamines in Alzheimer's disease patients with and without biological disease. Transl Psychiatry 12:151.

Hirata H, Aston-Jones G (1994) A novel long-latency response of locus coeruleus neurons to noxious stimuli: mediation by peripheral C-fibers. J Neurophysiol 71:1752–1761.

Hoogendijk WJ, Feenstra MG, Botterblom MH, Gilhuis J, Sommer IE, Kamphorst W, Eikelenboom P, Swaab DF (1999) Increased activity of surviving locus ceruleus neurons in Alzheimer's disease. Ann Neurol 45:82–91.

Iravani MM, Sadeghian M, Rose S, Jenner P (2014) Loss of locus coeruleus noradrenergic neurons alters the inflammatory response to LPS in substantia nigra but does not affect nigral cell loss. J Neural Transm (Vienna) 121:1493–1505.

Iro CM, Hamati R, El Mansari M, Blier P (2021) Repeated but not single administration of ketamine prolongs increases of the firing activity of norepinephrine and dopamine neurons. Int J Neuropsychopharmacol 24:570–579.

Jacobs HIL (2019) Focus on the blue locus for learning. Nat Hum Behav 3:1143–1144.

Jacobs HIL, Riphagen JM, Ramakers I, Verhey FRJ (2021a) Alzheimer's disease pathology: pathways between central norepinephrine activity, memory, and neuropsychiatric symptoms. Mol Psychiatry 26:897–906.

Jacobs HIL, Becker JA, Kwong K, Engels-Dominguez N, Prokopiou PC, Papp KV, Properzi M, Hampton OL, d'Oleire Uquillas F, Sanchez JS, Rentz DM, El Fakhri G, Normandin MD, Price JC, Bennett DA, Sperling RA, Johnson KA (2021b) In vivo and neuropathology data support locus coeruleus integrity as indicator of Alzheimer's disease pathology and cognitive decline. Sci Transl Med 13:eabj2511.

Johnson RD, Iuvone PM, Minneman KP (1987) Regulation of alpha-1 adrenergic receptor density and functional responsiveness in rat brain. J Pharmacol Exp Ther 242:842–849.

Jonsson G, Hallman H, Ponzio F, Ross S (1981) DSP4 (N-(2-chloroethyl)-N-ethyl-2-bromobenzylamine)–a useful denervation tool for central and peripheral noradrenaline neurons. Eur J Pharmacol 72:173–188.

Kelberman MA, Anderson CR, Chlan E, Rorabaugh JM, McCann KE, Weinshenker D (2022) Consequences of hyperphosphorylated tau in the locus coeruleus on behavior and cognition in a rat model of Alzheimer's disease. J Alzheimers Dis 86:1037–1059.

Kelly L, Seifi M, Ma R, Mitchell SJ, Rudolph U, Viola KL, Klein WL, Lambert JJ, Swinny JD (2021) Identification of intraneuronal amyloid beta oligomers in locus coeruleus neurons of Alzheimer's patients and their potential impact on inhibitory neurotransmitter receptors and neuronal excitability. Neuropathol Appl Neurobiol 47:488–505.

Kolisnyk B, Al-Onaizi M, Soreq L, Barbash S, Bekenstein U, Haberman N, Hanin G, Kish MT, Souza da Silva J, Fahnestock M, Ule J, Soreq H, Prado VF, Prado MAM (2017) Cholinergic surveillance over hippocampal RNA metabolism and Alzheimer's-like pathology. Cereb Cortex 27:3553–3567.

Kumbhare D, Holloway KL, Baron MS (2017) Parkinsonism and dystonia are differentially induced by modulation of different territories in the basal ganglia. Neuroscience 353:42–57.

Langfelder P, Zhang B, Horvath S (2008) Defining clusters from a hierarchical cluster tree: the dynamic tree cut package for R. Bioinformatics 24:719–720.

Levey AI, et al. (2022) A phase II study repurposing atomoxetine for neuroprotection in mild cognitive impairment. Brain 145:1924–1938.

Liu YU, Ying Y, Li Y, Eyo UB, Chen T, Zheng J, Umpierre AD, Zhu J, Bosco DB, Dong H, Wu L-J (2019) Neuronal network activity controls microglial process surveillance in awake mice via norepinephrine signaling. Nat Neurosci 22:1771–1781.

Logue MP, Growdon JH, Coviella IL, Wurtman RJ (1985) Differential effects of DSP-4 administration on regional brain norepinephrine turnover in rats. Life Sci 37:403–409.

Lustberg D, Tillage RP, Bai Y, Pruitt M, Liles LC, Weinshenker D (2020a) Noradrenergic circuits in the forebrain control affective responses to novelty. Psychopharmacology (Berl) 237:3337–3355.

Lustberg D, Iannitelli AF, Tillage RP, Pruitt M, Liles LC, Weinshenker D (2020b) Central norepinephrine transmission is required for stress-induced repetitive behavior in two rodent models of obsessive-compulsive disorder. Psychopharmacology (Berl) 237:1973–1987.

Lustberg DJ, Liu JQ, Iannitelli AF, Vanderhoof SO, Liles LC, McCann KE, Weinshenker D (2022) Norepinephrine and dopamine contribute to distinct repetitive behaviors induced by novel odorant stress in male and female mice. Horm Behav 144:105205.

Lyons WE, Fritschy JM, Grzanna R (1989) The noradrenergic neurotoxin DSP-4 eliminates the coeruleospinal projection but spares projections of the A5 and A7 groups to the ventral horn of the rat spinal cord. J Neurosci 9:1481–1489.

Madar IH, Sultan G, Tayubi IA, Hasan AN, Pahi B, Rai A, Sivanandan PK, Loganathan T, Begum M, Rai S (2021) Identification of marker genes in Alzheimer's disease using a machine-learning model. Bioinformation 17:348–355.

Martin-Iverson MT, Pisa M, Chan E, Fibiger HC (1982) Enhanced neophobia but normal plasma corticosterone levels in rats with dorsal noradrenergic bundle lesions. Pharmacol Biochem Behav 17:639–643.

Matschke LA, Komadowski MA, Stöhr A, Lee B, Henrich MT, Griesbach M, Rinné S, Geibl FF, Chiu WH, Koprich JB, Brotchie JM, Kiper AK, Dolga AM, Oertel WH, Decher N (2022) Enhanced firing of locus coeruleus neurons and SK channel dysfunction are conserved in distinct models of prodromal Alzheimer's disease. Sci Rep 12:3180.

Matsukawa M, Nakadate K, Ishihara I, Okado N (2003) Synaptic loss following depletion of noradrenaline and/or serotonin in the rat visual cortex: a quantitative electron microscopic study. Neuroscience 122:627–635.

McCall JG, Al-Hasani R, Siuda ER, Hong DY, Norris AJ, Ford CP, Bruchas MR (2015) CRH engagement of the locus coeruleus noradrenergic system mediates stress-induced anxiety. Neuron 87:605–620.

McIntyre CK, Miyashita T, Setlow B, Marjon KD, Steward O, Guzowski JF, McGaugh JL (2005) Memory-influencing intra-basolateral amygdala drug infusions modulate expression of Arc protein in the hippocampus. Proc Natl Acad Sci U S A 102:10718–10723.

McReynolds JR, Anderson KM, Donowho KM, McIntyre CK (2014) Noradrenergic actions in the basolateral complex of the amygdala modulate Arc expression in hippocampal synapses and consolidation of aversive and non-aversive memory. Neurobiol Learn Mem 115:49–57.

Mootha VK, et al. (2003) PGC-1alpha-responsive genes involved in oxidative phosphorylation are coordinately downregulated in human diabetes. Nat Genet 34:267–273.

Mulvey B, Bhatti DL, Gyawali S, Lake AM, Kriaucionis S, Ford CP, Bruchas MR, Heintz N, Dougherty JD (2018) Molecular and functional sex differences of noradrenergic neurons in the mouse locus coeruleus. Cell Rep 23:2225–2235.

Palmer AM, Francis PT, Bowen DM, Benton JS, Neary D, Mann DM, Snowden JS (1987) Catecholaminergic neurones assessed antemortem in Alzheimer's disease. Brain Res 414:365–375.

Peskind ER, Tsuang DW, Bonner LT, Pascualy M, Riekse RG, Snowden MB, Thomas R, Raskind MA (2005) Propranolol for disruptive behaviors in nursing home residents with probable or possible Alzheimer disease: a placebo-controlled study. Alzheimer Dis Assoc Disord 19:23–28.

Poe GR, Foote S, Eschenko O, Johansen JP, Bouret S, Aston-Jones G, Harley CW, Manahan-Vaughan D, Weinshenker D, Valentino R, Berridge C, Chandler DJ, Waterhouse B, Sara SJ (2020) Locus coeruleus: a new look at the blue spot. Nat Rev Neurosci 21:644–659.

Popova SN, Alafuzoff I (2013) Distribution of SLC10A4, a synaptic vesicle protein in the human brain, and the association of this protein with Alzheimer's disease-related neuronal degeneration. J Alzheimers Dis 37:603–610.

Prokopiou PC, Engels-Domínguez N, Papp KV, Scott MR, Schultz AP, Schneider C, Farrell ME, Buckley RF, Quiroz YT, El Fakhri G, Rentz DM, Sperling RA, Johnson KA, Jacobs HIL (2022) Lower novelty-related locus coeruleus function is associated with Aβ-related cognitive decline in clinically healthy individuals. Nat Commun 13:1571.

Raskind MA, Peskind ER, Holmes C, Goldstein DS (1999) Patterns of cerebrospinal fluid catechols support increased central noradrenergic responsiveness in aging and Alzheimer's disease. Biol Psychiatry 46:756–765.

Rommelfanger KS, Weinshenker D, Miller GW (2004) Reduced MPTP toxicity in noradrenaline transporter knockout mice. J Neurochem 91:1116–1124.

Rommelfanger KS, Edwards GL, Freeman KG, Liles LC, Miller GW, Weinshenker D (2007) Norepinephrine loss produces more profound motor deficits than MPTP treatment in mice. Proc Natl Acad Sci U S A 104:13804–13809.

Rorabaugh JM, Chalermpalanupap T, Botz-Zapp CA, Fu VM, Lembeck NA, Cohen RM, Weinshenker D (2017) Chemogenetic locus coeruleus activation restores reversal learning in a rat model of Alzheimer's disease. Brain 140:3023–3038.

Song S, Jiang L, Oyarzabal EA, Wilson B, Li Z, Shih YI, Wang Q, Hong JS (2019a) Loss of brain norepinephrine elicits neuroinflammation-mediated oxidative injury and selective caudo-rostral neurodegeneration. Mol Neurobiol 56:2653–2669.

Song S, Wang Q, Jiang L, Oyarzabal E, Riddick NV, Wilson B, Moy SS, Shih YI, Hong JS (2019b) Noradrenergic dysfunction accelerates LPS-elicited inflammation-related ascending sequential neurodegeneration and deficits in non-motor/motor functions. Brain Behav Immun 81:374–387.

Subramanian A, Tamayo P, Mootha VK, Mukherjee S, Ebert BL, Gillette MA, Paulovich A, Pomeroy SL, Golub TR, Lander ES, Mesirov JP (2005) Gene set enrichment analysis: a knowledge-based approach for interpreting genome-wide expression profiles. Proc Natl Acad Sci U S A 102:15545–15550.

Szot P, White SS, Greenup JL, Leverenz JB, Peskind ER, Raskind MA (2006) Compensatory changes in the noradrenergic nervous system in the locus ceruleus and hippocampus of postmortem subjects with Alzheimer's disease and dementia with Lewy bodies. J Neurosci 26:467–478.

Szot P, Miguelez C, White SS, Franklin A, Sikkema C, Wilkinson CW, Ugedo L, Raskind MA (2010) A comprehensive analysis of the effect of DSP4 on the locus coeruleus noradrenergic system in the rat. Neuroscience 166:279–291.

Szot P, Franklin A, Miguelez C, Wang Y, Vidaurrazaga I, Ugedo L, Sikkema C, Wilkinson CW, Raskind MA (2016) Depressive-like behavior observed with a minimal loss of locus coeruleus (LC) neurons following administration of 6-hydroxydopamine is associated with electrophysiological changes and reversed with precursors of norepinephrine. Neuropharmacology 101:76–86.

Takeuchi T, Duszkiewicz AJ, Sonneborn A, Spooner PA, Yamasaki M, Watanabe M, Smith CC, Fernández G, Deisseroth K, Greene RW, Morris RG (2016) Locus coeruleus and dopaminergic consolidation of everyday memory. Nature 537:357–362.

Tansey MG, Wallings RL, Houser MC, Herrick MK, Keating CE, Joers V (2022) Inflammation and immune dysfunction in Parkinson disease. Nat Rev Immunol 22:657–673.

Tao Y, Han Y, Yu L, Wang Q, Leng SX, Zhang H (2020) The predicted key molecules, functions, and pathways that bridge mild cognitive impairment (MCI) and Alzheimer's disease (AD). Front Neurol 11:233.

Thakur S, Dhapola R, Sarma P, Medhi B, Reddy DH (2022) Neuroinflammation in Alzheimer's disease: current progress in molecular signaling and therapeutics. Inflammation

Theofilas P, Ehrenberg AJ, Dunlop S, Di Lorenzo Alho AT, Nguy A, Leite REP, Rodriguez RD, Mejia MB, Suemoto CK, Ferretti-Rebustini REL, Polichiso L, Nascimento CF, Seeley WW, Nitrini R, Pasqualucci CA, Jacob Filho W, Rueb U, Neuhaus J, Heinsen H, Grinberg LT (2017) Locus coeruleus volume and cell population changes during Alzheimer's disease progression: a stereological study in human postmortem brains with potential implication for early-stage biomarker discovery. Alzheimers Dement 13:236–246.

Theron CN, de Villiers AS, Taljaard JJ (1993) Effects of DSP-4 on monoamine and monoamine metabolite levels and on beta adrenoceptor binding kinetics in rat brain at different times after administration. Neurochem Res 18:1321–1327.

Tillage RP, Sciolino NR, Plummer NW, Lustberg D, Liles LC, Hsiang M, Powell JM, Smith KG, Jensen P, Weinshenker D (2020) Elimination of galanin synthesis in noradrenergic neurons reduces galanin in select brain areas and promotes active coping behaviors. Brain Struct Funct 225:785–803.

Valentino RJ (1988) CRH effects on central noradrenergic neurons: relationship to stress. Adv Exp Med Biol 245:47–64.

van Hooren L, Vaccaro A, Ramachandran M, Vazaios K, Libard S, van de Walle T, Georganaki M, Huang H, Pietilä I, Lau J, Ulvmar MH, Karlsson MCI, Zetterling M, Mangsbo SM, Jakola AS, Olsson Bontell T, Smits A, Essand M, Dimberg A (2021) Agonistic CD40 therapy induces tertiary lymphoid structures but impairs responses to checkpoint blockade in glioma. Nat Commun 12:4127.

Vankov A, Hervé-Minvielle A, Sara SJ (1995) Response to novelty and its rapid habituation in locus coeruleus neurons of the freely exploring rat. Eur J Neurosci 7:1180–1187.

Wang Y, Musich PR, Serrano MA, Zou Y, Zhang J, Zhu MY (2014) Effects of DSP4 on the noradrenergic phenotypes and its potential molecular mechanisms in SH-SY5Y cells. Neurotox Res 25:193–207.

Weinshenker D (2018) Long road to ruin: noradrenergic dysfunction in neurodegenerative disease. Trends Neurosci 41:211–223.

Woitecki AM, Müller JA, van Loo KM, Sowade RF, Becker AJ, Schoch S (2016) Identification of synaptotagmin 10 as effector of NPAS4-mediated protection from excitotoxic neurodegeneration. J Neurosci 36:2561–2570.

Wolfman C, Abó V, Calvo D, Medina J, Dajas F, Silveira R (1994) Recovery of central noradrenergic neurons one year after the administration of the neurotoxin DSP4. Neurochem Int 25:395–400.

Zhang B, Horvath S (2005) A general framework for weighted gene co-expression network analysis. Stat Appl Genet Mol Biol 4: Article17.

Zhang X, Zuo DM, Yu PH (1995) Neuroprotection by R(-)-deprenyl and N-2-hexyl-N-methylpropargylamine on DSP-4, a neurotoxin, induced degeneration of noradrenergic neurons in the rat locus coeruleus. Neurosci Lett 186:45–48.

Zhao Y, Hu D, Wang R, Sun X, Ropelewski P, Hubler Z, Lundberg K, Wang Q, Adams DJ, Xu R, Qi X (2022) ATAD3A oligomerization promotes neuropathology and cognitive deficits in Alzheimer's disease models. Nat Commun 13:1121.

Zhou Y, Zhao WJ, Quan W, Qiao CM, Cui C, Hong H, Shi Y, Niu GY, Zhao LP, Shen YQ (2021) Dynamic changes of activated AHR in microglia and astrocytes in the substantia nigra-striatum system in an MPTP-induced Parkinson's disease mouse model. Brain Res Bull 176:174–183.